

Article

Response of Global Terrestrial Carbon Fluxes to Drought from 1981 to 2016

Qiaoning He^{1,2}, Weimin Ju^{2,3,*} and Xinchuan Li¹ ¹ School of Urban and Environmental Sciences, Huaiyin Normal University, Huaian 223300, China² International Institute for Earth System Sciences, Nanjing University, Nanjing 210023, China³ Jiangsu Provincial Key Laboratory of Geographic Information Science and Technology, Nanjing University, Nanjing 210023, China

* Correspondence: juweimin@nju.edu.cn

Abstract: Precipitation plays a dominant role in regulating terrestrial carbon fluxes. In concert with global warming, aridity has been increasing during recent decades in most parts of the world. How global terrestrial carbon fluxes respond to this change, however, is still unclear. Using a remote-sensing-driven, process-based model, the Boreal Ecosystem Productivity Simulator (BEPS), this study investigated the responses of global terrestrial carbon fluxes to meteorological drought, which were characterized by the standardized precipitation evapotranspiration index (SPEI). The results showed that the response of terrestrial carbon fluxes to drought exhibited distinguishable spatial heterogeneity. In most regions, terrestrial carbon fluxes responded strongly to drought. With an increase in annual water balance (annual precipitation minus annual potential evapotranspiration), the response of carbon fluxes to drought became weaker. The lagged time of terrestrial carbon fluxes responding to drought decreased with the increasing strength of carbon fluxes in response to drought. The sensitivity of terrestrial carbon fluxes to drought also showed noticeable spatial heterogeneity. With an increase in annual water balance, the sensitivity first increased and then decreased. Terrestrial carbon fluxes exhibited the highest sensitivity to drought in semi-arid areas.

Keywords: terrestrial carbon fluxes; response to drought; standardized precipitation evapotranspiration index; sensitivity; Boreal Ecosystem Productivity Simulator (BEPS) model

**Citation:** He, Q.; Ju, W.; Li, X.Response of Global Terrestrial Carbon Fluxes to Drought from 1981 to 2016. *Atmosphere* **2023**, *14*, 229. <https://doi.org/10.3390/atmos14020229>

Academic Editor: Mirela Voiculescu

Received: 17 December 2022

Revised: 12 January 2023

Accepted: 17 January 2023

Published: 23 January 2023



Copyright: © 2023 by the authors. Licensee MDPI, Basel, Switzerland. This article is an open access article distributed under the terms and conditions of the Creative Commons Attribution (CC BY) license (<https://creativecommons.org/licenses/by/4.0/>).

1. Introduction

Global terrestrial ecosystems play an important role in the carbon cycle and can absorb 25–30% of anthropogenic carbon emitted into the atmosphere [1,2]. Understanding the trend and variability of the terrestrial carbon fluxes is critical for predicting future climate change. Terrestrial carbon fluxes are affected by a number of factors, including climate [3–6], cyclones [7], atmospheric CO₂ fertilization [8], nitrogen deposition [9], land cover types, and land use change [10]. The intensity of terrestrial carbon flux is tightly coupled with the water cycle at different spatial and temporal scales [11–14]. Recent evidence has suggested that global semi-arid ecosystems play a significant role in the trend and variability of the land CO₂ sink [15,16]. The capacity of terrestrial ecosystems to sequester carbon is often dominated by water availability [17–19].

In concert with temperature increases, precipitation regimes have also changed since 1950 over a majority of land areas [20,21]. The impacts of changing precipitation conditions on plant productivity and terrestrial carbon fluxes have attracted considerable attentions from recent studies [22–30]. For example, based on field flux observations, remote sensing data, and model simulations, Ciais et al. [22] declared that the heat and drought observed in 2003 caused a 30% reduction in the continental-scale gross primary productivity (GPP) of Europe. This climatic extreme resulted in a strong anomalous net terrestrial carbon source in the atmosphere, offsetting the accumulation of four years of net ecosystem carbon sequestration by European terrestrial ecosystems. The GPP reductions in Eastern and

Western Europe were caused by rainfall deficit and extreme heat, respectively [31]. Based on the MODIS net primary productivity (NPP) product, Zhao and Running [25] found that drought caused global terrestrial NPP to decrease by $0.55 \text{ Pg C yr}^{-1}$ over the period from 2000 to 2009. Chen et al. [27] reported that NPP was positively and significantly related to water conditions at the global scale. Liu et al. [28] investigated the impact of drought on carbon sequestration in China's terrestrial ecosystems from 2000 to 2011 using the process-based Boreal Ecosystem Productivity Simulator (BEPS) driven by remotely sensed leaf area index (LAI). They found that national and regional total net ecosystem productivity (NEP) anomalies were correlated with the severity of drought indicated by using the mean annual standard precipitation index (SPI), especially in Northwest China, North China, Central China, and Southwest China. These findings together highlight the importance of understanding the response of the terrestrial carbon cycles to water conditions. However, few studies have focused on the relative response level of terrestrial carbon fluxes to drought.

Drought has both immediate and lagged effects on terrestrial carbon fluxes and vegetation growth [18,29,32–35]. Under drought conditions, both carbon assimilation and the amount of carbon released by ecosystem respiration (ER) usually decrease. The direct response of NEP to drought depends on the sensitivity of GPP and ER to the time of onset, severity, and duration of drought. During the initial stage of water depletion, vegetation is able to use deep soil water and maintain GPP at normal levels while ER starts to decrease as superficial soil layers dry out. NEP decreases marginally or even slightly increases. The further depletion of deep soil water significantly limits photosynthesis and results in a larger decrease in GPP than that in ER [31], and therefore in a decrease in NEP [36–38]. Based on long-term global AVHRR NDVI data, Vicente-Serrano et al. [29] reported that arid and humid biomes responded to drought at shorter time scales, while semi-arid and sub-humid ones responded to drought at longer time scales. A simulation using the BEPS model over the period from 2000 to 2011 by Liu et al. [28] showed that drought had short-term lagged impact on NEP in eastern humid and warm regions of China and a longer lagged effect on NEP in western cold and arid regions.

A central challenge for assessing the sensitivity of global terrestrial carbon fluxes to climate variability is that the dominant factors limiting terrestrial carbon sequestration have significant spatial variations [3,39–42]. Generally, in some humid regions and high latitudes, terrestrial carbon sequestration is dominantly regulated by solar radiation and temperature. The increase in precipitation is normally associated with a decrease in solar radiation [43] and consequently carbon sequestration might decrease [44]. A recent study suggested that ecosystem sensitivity to drought peaked over semi-arid ecosystems [45]. Meanwhile, Huxman et al. [19] reported that for aboveground net primary production, the highest sensitivity to interannual variations in rainfall was found at the driest sites, and that the wettest sites displayed the lowest sensitivity. The sensitivity of productivity to drought was found to be inversely related to mean annual precipitation [46]. Further studies are needed for deepening our insight into how global terrestrial carbon fluxes respond to drought.

Previous research has shown that drought may cause a decline in GPP without a change in vegetation greenness [47]. The immediate and lagged effects of drought on carbon fluxes and their sensitivities in different regions of the globe are still unclear. Therefore, this study aimed to quantify the response of global terrestrial carbon fluxes to drought over the time period from 1981 to 2016 by addressing three objectives: (1) to assess the maximum correlations between global terrestrial carbon fluxes and droughts; (2) to analyze the lagged effects of drought on global terrestrial carbon fluxes; and (3) to determine the changes in the sensitivity of carbon fluxes to drought in different regions of the globe. These objectives were achieved using global terrestrial carbon fluxes simulated using the BEPS model. Drought was assessed using the standardized precipitation evapotranspiration index (SPEI) [48]. SPEI is an extension of the widely used standardized precipitation index (SPI) [49]. It was designed to account for both precipitation and potential evapotranspi-

ration (PET) in determining drought. Unlike SPI, SPEI includes the effects of increased temperature on atmospheric water demand.

2. Materials and Methods

2.1. The Model Used to Simulate Global Carbon Fluxes

Global GPP, NPP, ER, and NEP were simulated using the BEPS model [50], which includes photosynthesis, energy balance, hydrological, and soil biogeochemical modules [51]. This model was initially developed to calculate NPP for the Canadian landmass at daily time steps. In recent years, it has been improved in many aspects and applied to simulate regional terrestrial carbon fluxes in China [28,52–54], North America [55–58], Europe [59], East Asia [60,61], and the globe [62–64]. Details about this model are described in references [53,56] and in the supplementary Text S1 in reference [63]. We only highlight the major methodologies of the model related to the calculation of global terrestrial GPP, NPP, and NEP here.

Canopy GPP is calculated as:

$$GPP = GPP_{sunlit}LAI_{sunlit} + GPP_{shaded}LAI_{shaded} \quad (1)$$

where GPP_{sunlit} and GPP_{shaded} are gross photosynthesis rates of sunlit and shaded leaves, respectively, and are calculated using the leaf level Farquhar model [65,66]; LAI_{sunlit} and LAI_{shaded} are the leaf area indexes of sunlit and shaded leaves, respectively.

NPP is calculated as the difference between GPP and autotrophic respiration:

$$NPP = GPP - R_g - R_m \quad (2)$$

where R_g and R_m denote growth respiration and maintenance respiration, respectively. The former is assumed to be 25% of GPP while the latter is calculated as a function of biomass, temperature, and the reference respiratory rate at a base temperature [56,67]:

$$R_m = \sum_{i=1}^1 R_{m,i} = \sum_{i=1}^1 M_i r_{m,i} Q_{10}^{(T-T_b)/10} \quad (3)$$

where M_i is the size of biomass carbon pool i ($i = 1, 2, 3, 4$, denoting leaf, stem, coarse root, and fine root carbon pools, respectively), $r_{m,i}$ is the respiration rate at a base temperature T_b , Q_{10} is the temperature sensitivity factor of maintenance respiration, and T is the temperature.

NEP is calculated as:

$$NEP = NPP - R_h \quad (4)$$

where R_h is the heterotrophic respiration occurring in nine litter and soil carbon pools (i.e., surface structural litter, surface metabolic litter, soil structural litter, soil metabolic litter, coarse woody litter, and surface microbial, soil microbial, slow, and passive carbon pools). R_h is calculated using algorithms adopted from the CENTURY model [68].

$$R_h = \sum_{j=1}^9 \tau_j k_j C_j \quad (5)$$

where τ_j is the respiration coefficient of pool j , k_j is the decomposition rate of pool j , and C_j is the size of pool j .

In the BEPS model, soil water conditions affect photosynthesis by regulating stomatal conductance and heterotrophic respiration by modifying the decomposition rate k_j . When soil water content is above field capacity, stomatal conductance and photosynthesis will not be limited. With the decrease in soil water content to wilting point, stomatal conductance will decrease to the minimum that limits photosynthesis. With the departure of soil water

content from the optima (at approximately 60% of saturation), the decomposition rates of soil carbon and litter pools will decrease.

2.2. Data Used to Drive the BEPS Model

The BEPS model was driven using a variety of input data, including spatially and temporally variable LAI, nitrogen deposition, standard meteorological data, spatially variable land cover data, and temporally variable CO₂ concentration data, as described below. The model was run for the period from 1901 to 2016. Only the simulated GPP, NPP, ER, and NEP over the period from 1981 to 2016 were used for analysis in this study since remotely sensed LAI only starts to become available in 1981.

2.2.1. Time Series of LAI during 1981–2016

LAI is an input to the BEPS model and critical for the simulation of carbon fluxes. The time series of LAI over the period from 1981 to 2016 was generated through fusion of LAI inverted from MODIS reflectance data and AVHRR GIMMS NDVI data [69]. LAI from 2000 to 2016 was first inverted from the MOD09A1 land surface reflectance and the associated illumination and view angles based on the GLOBCARBON LAI algorithm, which was developed using the four-scale geometric optical model. This algorithm explicitly considers the bidirectional reflectance distribution function (BRDF) effects on observed canopy reflectance. For the fusion of MODIS and AVHRR remote sensing data, the relationships between GIMMS NDVI and MODIS LAI were established pixel by pixel for their concurrent period (2000–2006) [69]. Then AVHRR LAI from 1981 to 2000 was generated using the same relationships. The spatial resolution of the LAI series is $0.072727^\circ \times 0.072727^\circ$ and temporal resolution varies from 16 days (1981 to 1999) to 8 days (2000 to 2016). In the simulation, these 16- and 8-days LAI values were interpolated to daily values. The BEPS model was driven using a climatological average LAI (1981–1989 data) for the period prior to satellite availability of LAI (1901 to 1980) and then the temporally variable LAI for the period from 1981 to 2016.

2.2.2. Global Nitrogen Deposition Data

Monthly global nitrogen deposition data at a $0.5^\circ \times 0.5^\circ$ resolution over the period from 1960 to 2009 were estimated using tropospheric NO₂ column density retrieved from the Global Ozone Monitoring Experiment (GOME) and from Scanning Imaging Absorption Spectrometer for Atmospheric Cartography (SCIAMACHY) sensors, meteorological data, and NO_x emission inventory data [70]. For the years 2010 to 2016, nitrogen data were extrapolated using estimated nitrogen data for the period from 2000 to 2009. For the period from 1901 to 1959, nitrogen data were extrapolated based on the rates of change of nitrogen deposition over the period from 1960 to 1969. The $0.5^\circ \times 0.5^\circ$ nitrogen deposition data were interpolated to $0.072727^\circ \times 0.072727^\circ$ resolution using a bilinear interpolation method [64].

2.2.3. Global Meteorological Data

The daily near-surface meteorological data, including daily maximum and minimum temperatures, relative humidity, solar radiation, and precipitation, were retrieved from the CRUNCEP V8.0 dataset, which extends the temporal coverage from 1901 to 2016 with a resolution of $0.5^\circ \times 0.5^\circ$. Relative humidity is required to force the BEPS model and was calculated from temperature, specific humidity, and pressure. The $0.5^\circ \times 0.5^\circ$ meteorological data were interpolated to $0.072727^\circ \times 0.072727^\circ$ resolution using a bilinear interpolation method.

2.2.4. Soil Data

Fractions of clay, silt, and sand were retrieved from the harmonized global soil database (http://www.fao.org/nr/lman/abst/lman_080701_en.htm, accessed on 18 June 2022) and used to determine model parameters, including the field capacity, porosity, wilting point, hydrological conductivity, etc.

2.3. Drought Assessment

Daily temperature and precipitation were used to calculate monthly SPEI values following Vicente-Serrano et al. [48]. Monthly potential evapotranspiration (PET) was computed using the Hargreaves–Sanani formula [71]. The monthly climatic water balance at different time scales was calculated as the difference between precipitation and PET and fitted with a three-parameter log-logistic probability distribution function used to calculate the standardized precipitation index (SPI) [49].

The cumulative probability distribution $F(x)$ of a water balance time series is given as:

$$F(x) = \left[1 + \left(\frac{\alpha}{x - \gamma} \right)^\beta \right]^{-1} \quad (6)$$

where α , β , and γ are scale, shape, and origin parameters, respectively.

Using the approximation of Abramowitz and Stegun [72], SPEI is calculated as:

$$\text{SPEI} = - \left(W - \frac{C_0 + C_1 W + C_2 W^2}{1 + d_1 W + d_2 W^2 + d_3 W^3} \right), \text{ for } 0 < F(x) \leq 0.5 \quad (7)$$

$$\text{SPEI} = + \left(W - \frac{C_0 + C_1 W + C_2 W^2}{1 + d_1 W + d_2 W^2 + d_3 W^3} \right), \text{ for } 0.5 < F(x) < 1 \quad (8)$$

where $C_0 = 2.515517$, $C_1 = 0.802853$, $C_2 = 0.010328$, $d_1 = 1.432788$, $d_2 = 0.189269$, and $d_3 = 0.001308$; W is determined as:

$$W = \sqrt{-2 \ln(F(x))} \quad \text{for } 0 < F(x) \leq 0.5 \quad (9)$$

$$W = \sqrt{-2 \ln(1 - F(x))} \quad \text{for } 0.5 < F(x) < 1 \quad (10)$$

In this study, SPEI was computed for each pixel at time scales from 1 to 24 months to capture the accumulated effects of water balance anomalies on terrestrial carbon fluxes. Positive SPEI values denote wet conditions while negative values indicate drought conditions.

2.4. Eddy Covariance Data

Eddy covariance data downloaded directly from the FLUXNET 2015 database (<http://fluxnet.fluxdata.org/data/fluxnet2015-dataset/>, accessed date: 15 August 2022) were used to validate the BEPS model. Sites with percentages of measured and good-quality gap-filled data more than 90% during the whole year were first selected. Then the sites with land cover types indicated by the site description in the FLUXNET database different from global land cover types adopted in the BEPS model were excluded from this validation. This resulted in a final 110 site-years used for validation of simulated monthly terrestrial carbon fluxes (Table 1).

2.5. Assessing Response of Terrestrial Carbon Fluxes to Drought

The response of terrestrial carbon fluxes to drought was assessed using Pearson's correlation coefficients of monthly GPP, NPP, ER, and NEP with SPEI. Terrestrial carbon fluxes might be enhanced by CO₂ fertilization and nitrogen deposition. To isolate these effects, monthly GPP, NPP, ER, and NEP were linearly detrended prior to the correlation analysis. The linear detrending was conducted by subtracting the linear trend from the original time series using the least squares method. For monthly analysis, individual 1- to 24-month-timescale SPEI series were correlated to monthly detrended GPP, NPP, ER, and NEP. For each month, 24 correlation coefficients were calculated for each carbon flux component. For each grid cell and each carbon flux, 288 (= 24 × 12) correlation coefficients were calculated.

Table 1. Site ID, latitude, longitude, vegetation types, and years of available data for the 22 FLUXNET sites used for validating BEPS model.

Site-ID	Vegetation Type	Latitude	Longitude	Years
AU-Cpr	SAV	−34.0021	140.5891	2011–2013
AU-Rob	EBF	−17.1175	145.6301	2014
AU-Wac	EBF	−37.4259	145.1878	2008
BR-Sa1	EBF	−2.8567	−54.9589	2002–2003
BR-Sa3	EBF	−3.018	−54.9714	2001,2003
CN-Cha	MF	42.4025	128.0958	2003
CN-Dan	GRA	30.4978	91.0664	2004–2005
CN-HaM	GRA	37.37	101.18	2003–2004
DE-Geb	CRO	51.1001	10.9143	2002–2014
DE-Kli	CRO	50.8929	13.5225	2006–2007,2010–2012,2014
FI-Hyy	ENF	61.8475	24.295	1997–1999,2001–2004, 2006–2009,2011–2014
GF-Guy	EBF	5.2788	−52.9249	2004–2014
IT-CA2	CRO	42.3772	12.026	2012–2013
MY-PSO	EBF	2.973	102.3062	2003,2007–2008
US-Blo	ENF	38.8953	−120.6328	2000
US-CRT	CRO	41.6285	−83.3471	2011–2013
US-MMS	DBF	39.3232	−86.4131	2002–2006,2008–2009, 2012–2014
US-Me2	ENF	44.4523	−121.5574	2005,2009
US-Me5	ENF	44.4372	−121.5668	2001
US-NR1	ENF	40.0329	−105.5464	2000–2014
US-Ne3	CRO	41.1797	−96.4397	2002–2012
US-SRC	OSH	31.9083	−110.8395	2009–2011

For each carbon flux, we then calculated a response measure defined as the maximum value from the 288 correlation coefficients. We also calculated a sensitivity measure defined as the change in monthly carbon flux per unit change in monthly SPEI for each pixel, where monthly carbon flux and monthly SPEI time scale were corresponded to the month and time scale when the maximum correlation coefficient was identified. The sensitivity of carbon flux to drought was quantified as the slope of the linear regression between carbon flux and SPEI. Before computing the sensitivity, monthly carbon fluxes were also linearly detrended to avoid spurious correlations.

3. Results

3.1. Validation of Simulated Monthly Terrestrial Carbon Fluxes

The simulated monthly GPP, ER, and NEP were compared with eddy covariance tower data from the FLUXNET 2015 database across different ecosystem types (Figure 1). The model captured 71%, 73%, and 23% of variation in monthly GPP, ER, and NEP for 1320 site-months measurements at eddy covariance sites, respectively, indicating the applicability of the BEPS model in estimating carbon fluxes for different ecosystems across the globe, although in some cases the model underestimated or overestimated the measured values.

To verify whether the performance of the BEPS model differs in months with and without drought, all site-months were classified into two groups according to values of SPEI. The coefficient of determinations, R^2 of simulated GPP, ER, and NEP against tower-based values were 0.70, 0.74, and 0.21 for 687 site-months with drought conditions (SPEI < 0) (red squares in Figure 1), respectively. As to the 633 site-months without drought (SPEI > 0) (blue circles in Figure 1), the R^2 values of simulated GPP, ER, and NEP against tower-based values were 0.73, 0.73, and 0.26, respectively. Therefore, whether in drought or non-drought conditions, the BEPS model could simulate the terrestrial carbon fluxes with good accuracy, and more importantly, the simulation ability was similar.

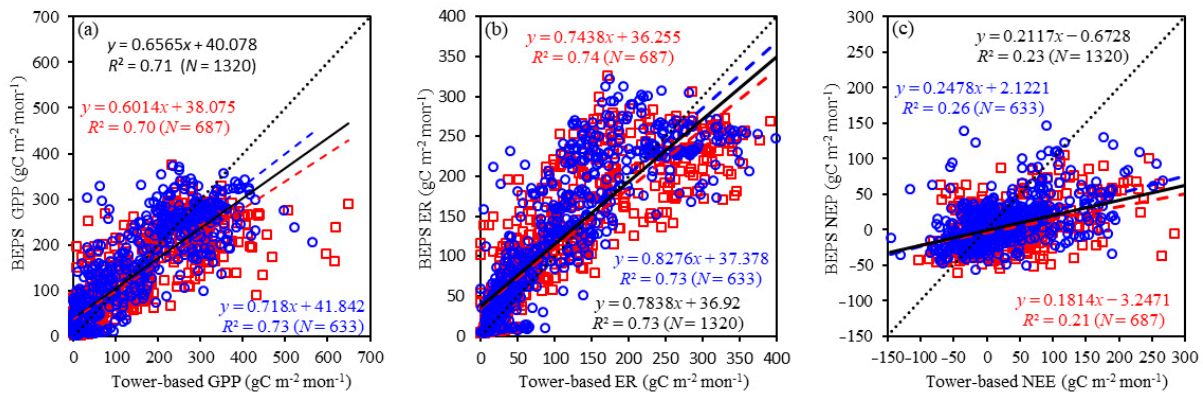


Figure 1. Comparison of simulated monthly GPP (a), ER (b) and NEP (c) with data compiled from FLUXNET2015 database. The black solid line is the regression line for all data while the dash line is the 1:1 line. The red dotted line is the regression line for data in drought months (monthly SPEI-1 < 0), and the blue dotted line is the regression line for data in wet months (monthly SPEI-1 > 0).

3.2. Spatial Variations of the Response of Terrestrial Carbon Fluxes to Drought

Global maps with maximum correlation coefficients between the monthly terrestrial carbon fluxes and the SPEI were generated to assess the spatial patterns of carbon fluxes' responses to drought (Figure 2). The significant positive correlations of carbon fluxes with SPEI (red colored areas) mainly occurred in the southern hemisphere and at low to middle latitudes of the northern hemisphere. This indicated that carbon fluxes decreased significantly in drought months in these areas. At high latitudes of the northern hemisphere, correlations of carbon fluxes with SPEI were positive, but weaker. In abnormal wet months, terrestrial carbon fluxes might decrease correspondingly in these regions. These findings revealed differential responses of terrestrial carbon fluxes to drought in different regions.

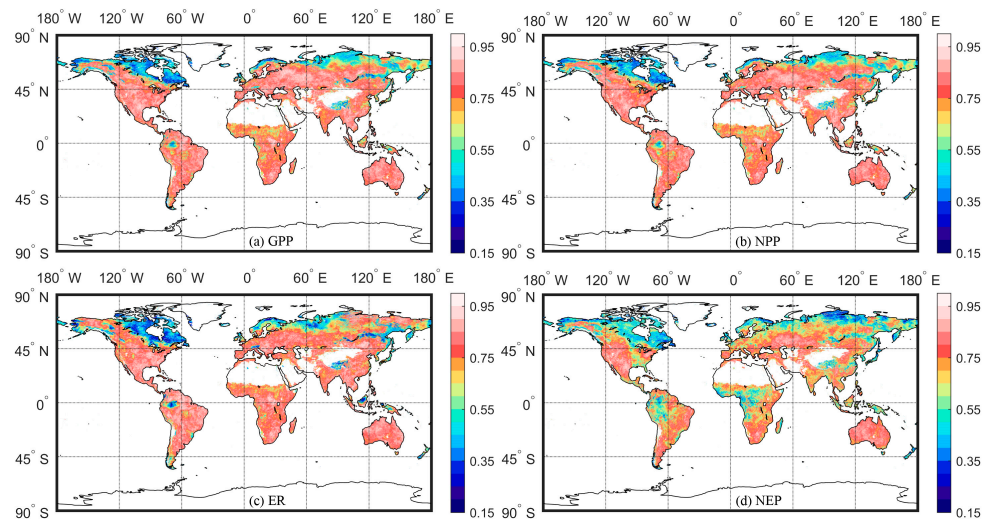


Figure 2. Spatial distributions of the correlations between detrended SPEI and monthly GPP (a), NPP (b), ER (c), and NEP (d) for the period 1981–2016. The values represent the maximum correlation recorded for each pixel, independent of the month of the year and the SPEI time scale. The maximum correlation coefficient was selected from the calculated 288 (= 24 × 12) correlation coefficients. Desert, sea, and ice areas are depicted in white.

The maximum correlation coefficients analysis in this study showed that terrestrial GPP, NPP, and ER showed similar correlograms with drought throughout many regions across the globe, with the exception of the high latitudes of the northern hemisphere, where ER had a different spatial pattern compared to GPP and NPP (Figure 2a–c). The areas with

low values for the maximum correlation coefficients of monthly GPP, NPP and ER with SPEI were mainly located in northern North America, northern Eurasia, the Qinghai–Tibet Plateau, the Amazon Basin, and Southeast Asia. As for the other regions of the globe, the maximum correlation coefficients were generally above 0.75, indicating that the higher the degree of wetness, the stronger the terrestrial photosynthesis and respiration; and, in contrast, the higher the degree of drought, the lower the terrestrial photosynthesis and respiration of terrestrial ecosystems.

Compared to those for GPP, NPP, and ER, the maximum correlation coefficients between NEP and SPEI were generally lower and had higher degrees of spatial heterogeneity. NEP was jointly controlled by GPP and ER, which could decrease concurrently in drought conditions with similar magnitude. However, the relatively higher reductions in ER or GPP would indicate a weaker or stronger response of NEP to drought.

3.3. Characteristics of Lagged Response of the Terrestrial Carbon Fluxes to Drought

The responses of terrestrial carbon fluxes to drought were lagged at different temporal scales in different regions (Figure 3). In cold regions, such as northern Canada, central and eastern Eurasia, and the Qinghai–Tibet Plateau, the response of terrestrial carbon fluxes to drought lagged for a relatively longer period, mostly above 10 months. In humid regions, such as the eastern United States, western Europe, the Amazon basin, central and western Africa, and southeastern China, the response of terrestrial carbon fluxes to drought lagged for a relatively shorter period, generally less than 4 months. In arid and semi-arid regions, such as the western United States, southern South America, southern Europe, northeastern China, northern Africa, and western Australia, the lagged time for terrestrial carbon fluxes in response to drought ranged from 6 to 10 months. Overall, the lagged time of terrestrial carbon fluxes responding to drought was longer in areas with weaker responses of carbon fluxes to drought than in areas with stronger responses of carbon fluxes to drought.

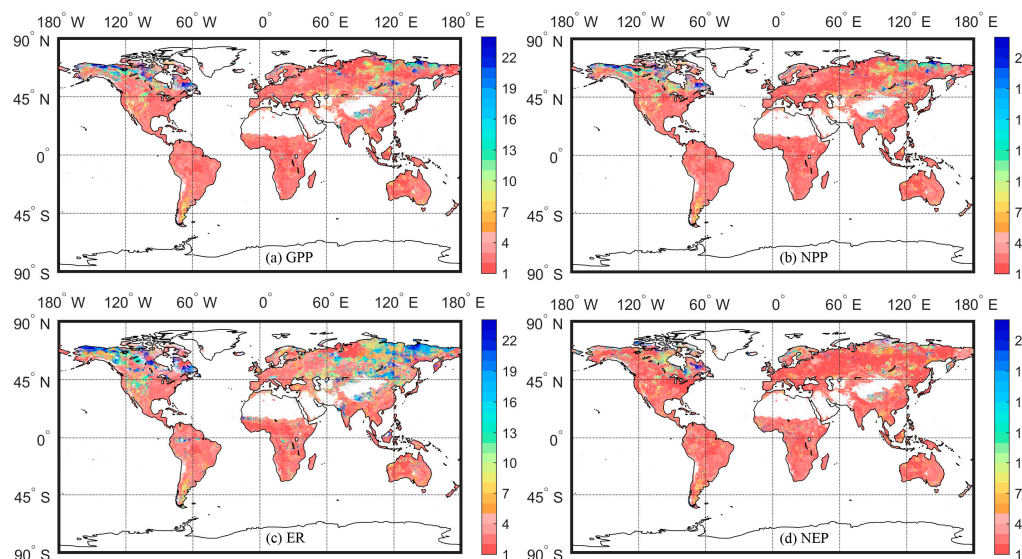


Figure 3. Lagged months of the strongest response of terrestrial GPP (a), NPP (b), ER (c), and NEP (d) to drought. Areas with no significant correlations between carbon fluxes and SPEI, and areas with desert, sea, and ice, are depicted in white.

GPP, NPP and NEP had similar spatial distributions of lagged time in response to drought, while the lagged time of ER in response to drought differed from GPP, NPP, and NEP (Figure 3). This difference was partly reflected in the increased area of regions with longer lagged months to drought, and partly in the higher spatial heterogeneity of ER in response to drought. In arid and semi-arid regions such as the western United States, southern South America, western India, southern Africa, and western Australia, the lagged months of ER in response to drought were significantly longer than those of GPP, NPP,

and NEP. In cold regions, such as northern Eurasia, northern North America, and the Qinghai–Tibet Plateau, the lagged months of ER in response to drought were also longer.

Globally, the lag effects of drought on GPP, NPP, ER, and NEP were almost identical with longer time scales in semi-arid and semi-humid regions and shorter time scales in arid and humid areas (Figures 3 and 4). In areas with a negative annual water balance averaged over the period from 1981 to 2016, the lagged time of terrestrial carbon fluxes in response to drought increased with increasing annual water balance. In contrast, in areas with a positive annual water balance, the lagged time of terrestrial carbon fluxes in response to drought decreased with the increasing annual water balance.

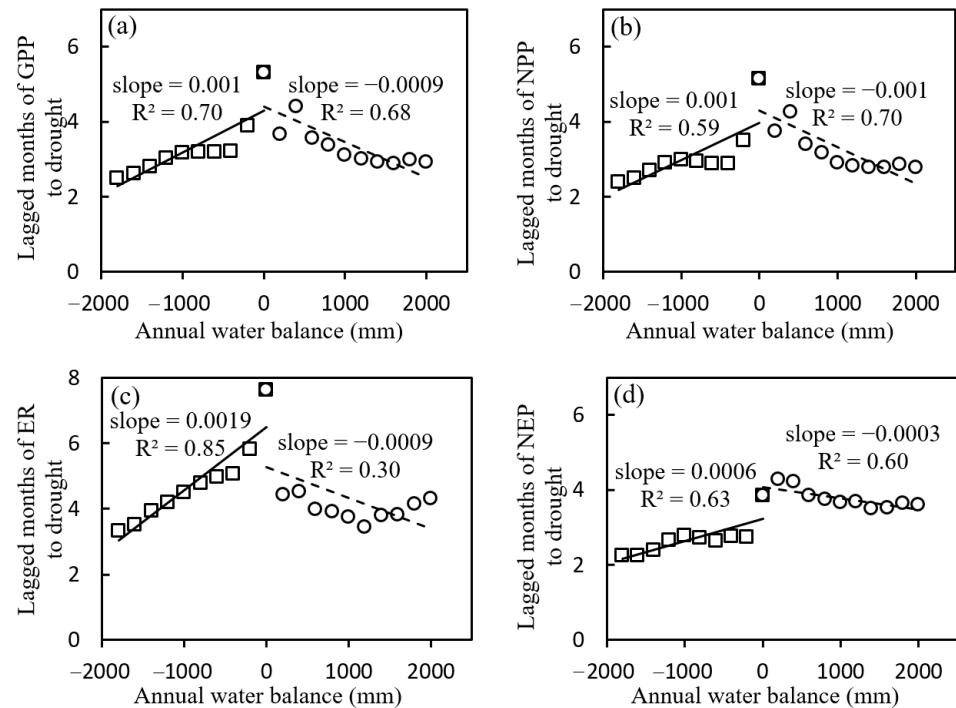


Figure 4. Changes of lagged time (month) for response of terrestrial GPP (a), NPP (b), ER (c), and NEP (d) to drought with annual water balance averaged over the period from 1981 to 2016.

3.4. Spatial Patterns of Sensitivity of the Terrestrial Carbon Fluxes to Drought

Based on the identified lagged time scales of SPEI, the sensitivity of carbon fluxes to drought was calculated for each grid cell for the month in which the carbon fluxes and the SPEI were found to have the highest correlation coefficients (Figure 5). The sensitivity of terrestrial carbon fluxes to drought was high in the eastern United States, most of Europe, East Asia, and eastern South America, and was low in the high latitudes of the Northern Hemisphere, the western United States, northern and southern Africa, Central Asia, and western Australia. This could be attributed to differences in the size of terrestrial carbon fluxes themselves and differences in the responses of carbon fluxes to drought in different regions.

In order to remove the influence of the state of terrestrial carbon fluxes in different regions, the sensitivity was further calculated based on the detrended and normalized terrestrial carbon fluxes ($F_{\text{normalized}} = (F - F_{\text{mean}})/F_{\text{std}}$; $F_{\text{normalized}}$ and F are the normalized and detrended monthly carbon fluxes; F_{mean} and F_{std} are the mean and standard deviation of F over the study period) (Figure 6). As a result, the sensitivity of terrestrial carbon fluxes to drought showed an alternative spatial pattern. In general, the sensitivity was higher at low and middle latitudes in the Northern Hemisphere and in the Southern Hemisphere, while the sensitivity values were relatively lower at high latitudes in the Northern Hemisphere.

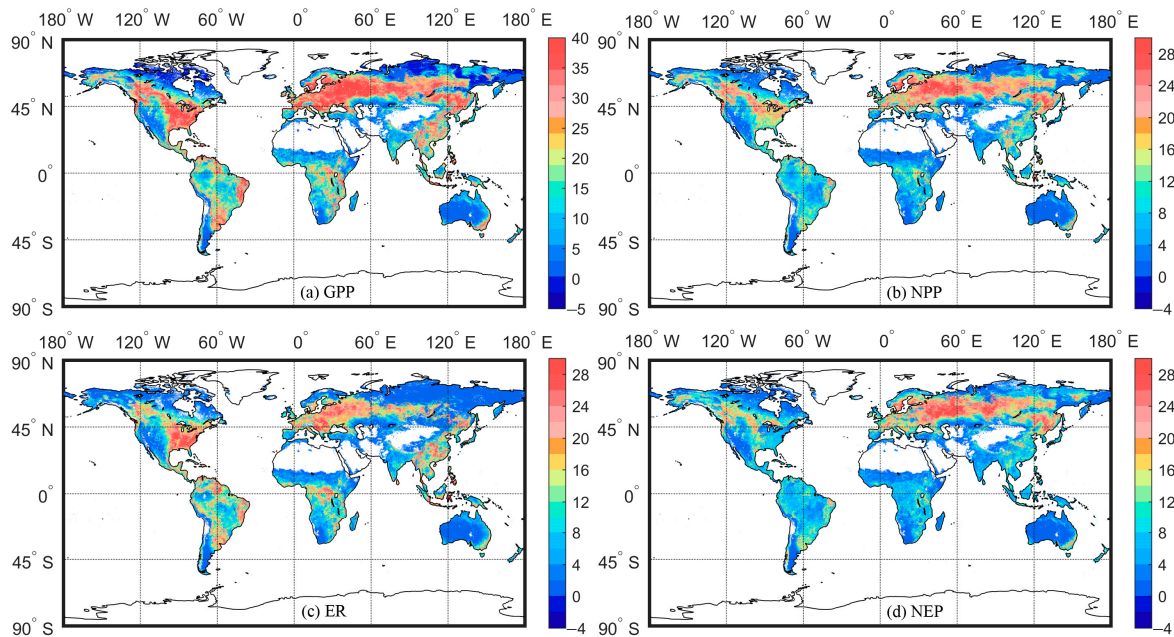


Figure 5. The sensitivity ($\text{g C m}^{-2} \text{ mon}^{-1} / \text{SPEI}$) of terrestrial GPP (a), NPP (b), ER (c), and NEP (d) to drought. Areas with no significant correlations of carbon fluxes with SPEI, and areas with desert, sea, and ice, are depicted in white.

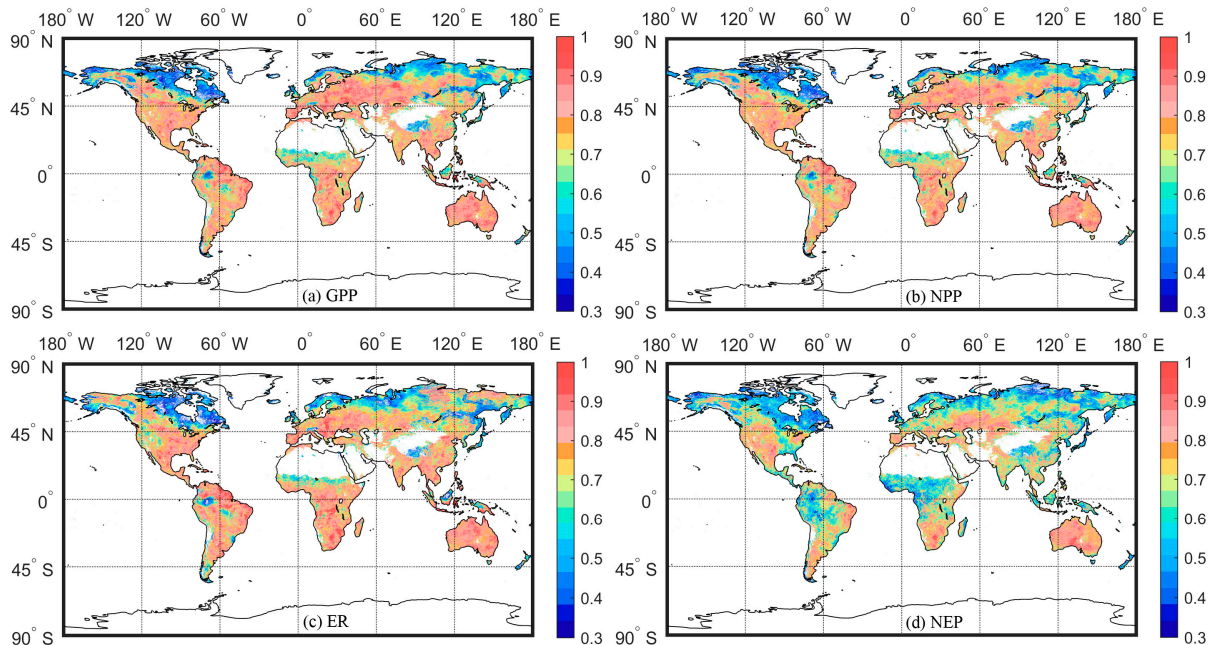


Figure 6. Spatial distributions of the sensitivity of detrended and normalized terrestrial GPP (a), NPP (b), ER (c), and NEP (d) to drought. Areas with no significant correlations, and areas with desert, sea, and ice, are depicted in white.

3.5. Changes in the Sensitivity of Terrestrial Carbon Fluxes to Drought with Wetness Conditions

To further explore the dependency of the sensitivity of terrestrial carbon fluxes to drought on the degree of water condition, the change in the sensitivity of regional monthly carbon fluxes to drought with regional mean annual water balance averaged over the period from 1981 to 2016 was analyzed (Figure 7). The sensitivity of terrestrial carbon fluxes to drought was low in arid and humid areas, while in semi-arid and semi-humid areas the sensitivity of terrestrial carbon fluxes to drought was high. In areas with negative annual

water balance, the sensitivity of terrestrial carbon fluxes to drought increased significantly with increasing annual water balance. In contrast, in areas with positive annual water balance, the sensitivity of terrestrial carbon fluxes to drought decreased with increasing annual water balance, except for ER. Overall, with the increase in annual water balance, the sensitivity first increased and then decreased. Terrestrial carbon fluxes exhibited the highest sensitivity to drought in semi-arid areas.

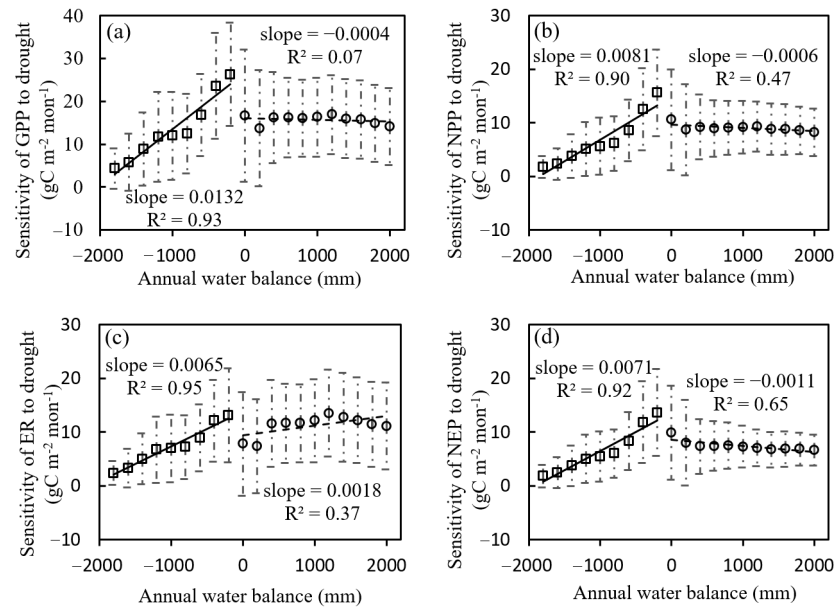


Figure 7. Changes in the sensitivity of terrestrial GPP (a), NPP (b), ER (c), and NEP (d) to drought with regional mean annual water balance averaged over the period from 1981 to 2016.

4. Discussion

4.1. Uncertainties of Simulated Terrestrial Carbon Fluxes and Drought Assessment

In this study, the BEPS model was driven using remotely sensed LAI to simulate carbon fluxes at daily time steps. Owing to drawbacks in model structure, parameterization, and inputs, there were definitely some uncertainties in the simulated carbon fluxes. For example, by not accounting for the horizontal movement of soil water, the model might overestimate/underestimate the drought-induced decrease in carbon fluxes in lowlands/uplands. NEP is affected by a number of factors including climate change, land use change, and disturbances [4,28]. Land cover and land use changes could significantly influence terrestrial carbon fluxes [24,73]. In this study, a static land cover map was used to drive the BEPS model. The impacts of land cover and land use changes as well as disturbances on carbon fluxes were only partially captured through remotely sensed LAI. This simplification was another source of uncertainty in the simulated carbon fluxes.

LAI is an important input into the BEPS model and an important determinant for the temporal trends of simulated carbon fluxes [64]. The LAI during 1981–2016 used here was generated through fusing AVHRR NDVI and MODIS data inverted pixel by pixel [69]. Overall, these two datasets are consistent. However, their consistency was poor for some regions, which might cause uncertainties in the temporal trends of simulated carbon fluxes and their responses to drought.

Moreover, we should keep in mind that the drought identified by SPEI represented a change in water balance over the year relative to the multi-year mean over the study period. The SPEI is a standardized variate over the conditions that are normal at a given site, which can be quantitatively compared across sites with very different climatology; that is, a drought of SPEI equal to -1 in a tropical forest region will be very different from a drought of SPEI equal to -1 in the Sahel region, but both situations are comparable because they represent the same degree of deviation from the normal conditions at each site [74].

Therefore, a year with low SPEI in a wet area may not necessarily cause vegetation water stress and may still be wetter than a year with high SPEI in a dry region [63]. In this case, SPEI is unable to capture ecological drought which affects vegetation productivity [75,76].

4.2. Spatial Patterns of Impacts of Drought on Carbon Fluxes

Previous studies have indicated that GPP responds to changes in temperature, precipitation, and/or radiation. The relative importance of these meteorological factors varies with regions [3,77]. In this study, interannual variations of simulated annual GPP were generally positively correlated with SPEI, especially in regions south of 45°N. Vicente-Serrano et al. [29] reported that vegetation activity and growth were significantly positively correlated with SPEI over 72% of global vegetated land areas. Based on flux observations in China, Yu et al. [78] found that tower-based GPP increased with annual precipitation and mean annual temperature at low latitudes. In the BEPS model, NPP is calculated as the difference between GPP and autotrophic respiration, which comprises growth and maintenance respiration. The former was calculated as a proportion of GPP and the latter was calculated as a function of biomass, temperature, and reference respiratory rate. Consequently, GPP is the dominant determinant of NPP. Therefore, simulated GPP and NPP showed similar spatial patterns in response to drought.

NEP is the balance between GPP and ER. In most regions of the globe, soil water content is seldom above field capacity and drought might cause both GPP and ER to decrease. As a consequence, GPP and NEP show similar sensitivity to drought, as has been reported by Guo-Dong [79] and Xu et al. [80]. At middle and high latitudes of the northern hemisphere, such as the Eurasia region, simulated NEP was less susceptible to drought than GPP and NPP (Figure 2). In this region, soil organic matter is rich and soil water content is often between field capacity and wilting point. Mild or moderate drought might significantly enhance heterotrophic respiration and limit GPP to a lesser extent. Therefore, NEP is less sensitive to drought in comparison with GPP and NPP in these regions.

At high latitudes of the northern hemisphere, temperature and radiation play more important roles in regulating GPP and NPP [3]. The increase in precipitation is normally accompanied by decreases in temperature and radiation, and consequently causes GPP and NPP to decrease. The lower correlations between SPEI and simulated carbon fluxes in this study further confirm that abnormal wetness may induce the terrestrial carbon fluxes to decrease in this region.

4.3. Lagged Effects of Precipitation Anomalies on Carbon Fluxes

Understanding the direct and lagged responses of terrestrial productivity to drought is crucial for assessing the effects of climate change on terrestrial ecosystems. The remotely sensed NDVI has been used as an indicator of terrestrial ecosystem productivity [81,82], for investigating both direct and lagged effects of climatic change on vegetation activity and growth. Ji and Peters [83] found that the NDVI had the best correlation with the 3-month SPI, and the best NDVI-SPI relationship occurred in regions with low soil water-holding capacity. Using the NDVI and SPEI data, Vicente-Serrano et al. [29] reported responses of global biomes to drought. They concluded that both arid and humid biomes responded to drought at short time scales and semi-arid and sub-humid biomes responded to drought at long time scales. The overall picture of our simulated lagged time scales was remarkably similar to this previous analysis.

The lagged months at which terrestrial carbon fluxes respond to drought was also found to vary in different regions in this study. From the point of the world's climate type, the lagged time scales of drought impacting carbon fluxes are relatively short in tropical climate areas and long in cold climate regions. Similar findings have been reported in a study that used vegetation indices, tree-ring growth data, and GPP [29,33]. Based on eddy covariance flux data, Zhang et al. [84] recently reported that temperate grassland ecosystems responded to climatic factors (i.e., net radiation, precipitation, and soil water

content) at longer time scales while alpine ecosystems showed a less obvious time-lagged response to these factors.

4.4. Dependence of the Sensitivity of Terrestrial Carbon Fluxes to Drought on Climate Conditions

An additional finding of this study was that sensitivity of the terrestrial carbon fluxes to drought was the highest in semi-arid areas. This is consistent with the peaked hydroclimatic sensitivity over semi-arid regions found by Ma et al. [45] using an enhanced vegetation index and SPEI. However, by quantifying reductions in above-ground net primary production, Knapp et al. [46] reported that drought sensitivity generally decreased with increasing mean annual precipitation. Our results partly agreed with the above study, since in areas with negative annual water balance, the sensitivity of terrestrial carbon fluxes to drought increased significantly with increasing annual water balance, but in areas with positive annual water balance, the sensitivity of terrestrial carbon fluxes to drought decreased with increasing annual water balance, except for ER.

Although sensitivity of the terrestrial carbon fluxes generally increased with increasing annual water balance, and then decreased with increasing annual water balance, there was large heterogeneity in different climate conditions, especially in humid regions (indicated by the error bars in Figure 7). This may be attributed to the different climatic constraints in these areas. For instance, in the temperate humid regions of Asia, radiation played a more important role in explaining productivity variability [3], while in the temperate humid regions of Oceania, water was the most important limiting factor [3]. It is important to note that different terrestrial ecosystem growth controlled by different climatic constraints may respond differently during wet or drought conditions.

5. Conclusions

With the remote-sensing-driven BEPS model, this study investigated the responses of global carbon fluxes to drought, which were indicated by the maximum correlation coefficients between terrestrial carbon fluxes and SPEI, and by the sensitivity of terrestrial carbon fluxes to drought. The main findings were:

- (1) The maximum correlation coefficients between terrestrial carbon fluxes and SPEI varied spatially. In southern North America, central Eurasia, East Asia, most of South America, most of Africa, and Australia, terrestrial carbon fluxes responded strongly to drought. In northern North America, northeastern Eurasia, the Tibetan Plateau, the Amazon Basin, and the tropical rainforest regions of Southeast Asia, the response of carbon fluxes to drought was weaker, and in abnormal wet years, carbon fluxes might decrease. Overall, with the increase in positive annual water balance, the response of carbon fluxes to drought became weaker.
- (2) The time scales at which the strongest responses of carbon fluxes to drought were discovered were various in the different regions. Drought had short-term lagged effects on carbon fluxes in arid and humid climate areas. In contrast, carbon fluxes in semi-arid and semi-humid areas responded to drought at relatively longer time scales.
- (3) The sensitivity of monthly carbon fluxes to drought differed spatially. In areas with a negative annual water balance, the sensitivity of terrestrial carbon fluxes in response to drought increased with increasing annual water balance. In areas with a positive annual water balance, there was a slight decrease trend with increasing annual water balance.

Author Contributions: All of the authors contributed significantly to this manuscript. Conceptualization, W.J.; data curation, Q.H. and W.J.; methodology, Q.H. and W.J.; writing—original draft, Q.H., W.J., and X.L. All authors have read and agreed to the published version of the manuscript.

Funding: This research was funded by the National Natural Science Foundation of China (42141005, 41801075) and the Jiangsu University Philosophy and Social Science Research Fund (2018SJA1611).

Institutional Review Board Statement: Not applicable.

Informed Consent Statement: Not applicable.

Data Availability Statement: Not applicable.

Acknowledgments: This work used eddy covariance data acquired and shared by the FLUXNET community, including these networks: AmeriFlux, AfriFlux, AsiaFlux, CarboAfrica, CarboEuropeIP, CarboItaly, CarboMont, ChinaFlux, Fluxnet-Canada, GreenGrass, ICOS, KoFlux, LBA, NECC, OzFlux-TERN, TCOS-Siberia, and USCCC. The ERA-Interim reanalysis data were provided by ECMWF and processed by LSCE. The FLUXNET eddy covariance data processing and harmonization was carried out by the European Fluxes Database Cluster, the AmeriFlux Management Project, and the Fluxdata project of FLUXNET, with the support of the CDIAC, the ICOS Ecosystem Thematic Centre, and the OzFlux, ChinaFlux, and AsiaFlux offices.

Conflicts of Interest: The authors declare no conflict of interest.

References

1. Ciais, P.; Sabine, C.; Bala, G.; Bopp, L.; Brovkin, V.; Canadell, J.; Chhabra, A.; DeFries, R.; Galloway, J.; Heimann, M.; et al. Carbon and Other Biogeochemical Cycles. In *Climate Change 2013: The Physical Science Basis. Contribution of Working Group I to the Fifth Assessment Report of the Intergovernmental Panel on Climate Change*; Cambridge University Press: Cambridge, UK; New York, NY, USA, 2013; pp. 465–570.
2. Le Quéré, C.; Raupach, M.R.; Canadell, J.G.; Marland, G.; Bopp, L.; Ciais, P.; Conway, T.J.; Doney, S.C.; Feely, R.A.; Foster, P.; et al. Trends in the sources and sinks of carbon dioxide. *Nat. Geosci.* **2009**, *2*, 831–836. [[CrossRef](#)]
3. Nemani, R.R.; Keeling, C.D.; Hashimoto, H.; Jolly, W.M.; Piper, S.C.; Tucker, C.J.; Myneni, R.B.; Running, S.W. Climate-Driven Increases in Global Terrestrial Net Primary Production from 1982 to 1999. *Science* **2003**, *300*, 1560–1563. [[CrossRef](#)] [[PubMed](#)]
4. Heimann, M.; Reichstein, M. Terrestrial ecosystem carbon dynamics and climate feedbacks. *Nature* **2008**, *451*, 289–292. [[CrossRef](#)] [[PubMed](#)]
5. Piao, S.; Sitch, S.; Ciais, P.; Friedlingstein, P.; Peylin, P.; Wang, X.; Ahlström, A.; Anav, A.; Canadell, J.G.; Cong, N.; et al. Evaluation of terrestrial carbon cycle models for their response to climate variability and to CO₂ trends. *Glob. Chang. Biol.* **2013**, *19*, 2117–2132. [[CrossRef](#)] [[PubMed](#)]
6. Ukkola, A.M.; De Kauwe, M.G.; Roderick, M.L.; Burrell, A.; Lehmann, P.; Pitman, A.J. Annual precipitation explains variability in dryland vegetation greenness globally but not locally. *Glob. Chang. Biol.* **2021**, *27*, 4367–4380. [[CrossRef](#)]
7. Hutley, L.; Beringer, J. Disturbance and Climatic Drivers of Carbon Dynamics of a North Australian Tropical Savanna. In *Ecosystem Function in Savannas: Measurement and Modeling at Landscape to Global Scales*; CRC Press: Boca Raton, FL, USA, 2010; pp. 57–75. [[CrossRef](#)]
8. Wang, S.; Zhang, Y.; Ju, W.; Chen, J.M.; Ciais, P.; Cescatti, A.; Sardans, J.; Janssens, I.A.; Wu, M.; Berry, J.A.; et al. Recent global decline of CO₂ fertilization effects on vegetation photosynthesis. *Science* **2020**, *370*, 1295–1300. [[CrossRef](#)]
9. Albani, M.; Medvigy, D.; Hurtt, G.C.; Moorcroft, P.R. The contributions of land-use change, CO₂ fertilization, and climate variability to the Eastern US carbon sink. *Glob. Chang. Biol.* **2006**, *12*, 2370–2390. [[CrossRef](#)]
10. Houghton, R.A.; Hackler, J.L. Changes in terrestrial carbon storage in the United States. 1: The roles of agriculture and forestry. *Glob. Ecol. Biogeogr.* **2000**, *9*, 125–144. [[CrossRef](#)]
11. Beringer, J.; Hacker, J.; Hutley, L.B.; Leuning, R.; Arndt, S.K.; Amiri, R.; Bannehr, L.; Cernusak, L.A.; Grover, S.; Hensley, C.; et al. SPECIAL—Savanna Patterns of Energy and Carbon Integrated across the Landscape. *Bull. Am. Meteorol. Soc.* **2011**, *92*, 1467–1485. [[CrossRef](#)]
12. Li, W.; Migliavacca, M.; Forkel, M.; Walther, S.; Reichstein, M.; Orth, R. Revisiting Global Vegetation Controls Using Multi-Layer Soil Moisture. *Geophys. Res. Lett.* **2021**, *48*, e92856. [[CrossRef](#)]
13. Marcolla, B.; Migliavacca, M.; Rödenbeck, C.; Cescatti, A. Patterns and trends of the dominant environmental controls of net biome productivity. *Biogeosciences* **2020**, *17*, 2365–2379. [[CrossRef](#)]
14. Wang, M.; Wang, S.; Zhao, J.; Ju, W.; Hao, Z. Global positive gross primary productivity extremes and climate contributions during 1982–2016. *Sci. Total Environ.* **2021**, *774*, 145703. [[CrossRef](#)]
15. Ahlström, A.; Raupach, M.R.; Schurgers, G.; Smith, B.; Arneth, A.; Jung, M.; Reichstein, M.; Canadell, J.G.; Friedlingstein, P.; Jain, A.K.; et al. The dominant role of semi-arid ecosystems in the trend and variability of the land CO₂ sink. *Science* **2015**, *348*, 895–899. [[CrossRef](#)] [[PubMed](#)]
16. Poulter, B.; Frank, D.; Ciais, P.; Myneni, R.B.; Andela, N.; Bi, J.; Broquet, G.; Canadell, J.G.; Chevallier, F.; Liu, Y.Y.; et al. Contribution of semi-arid ecosystems to interannual variability of the global carbon cycle. *Nature* **2014**, *509*, 600–603. [[CrossRef](#)]
17. Reichstein, M.; Papale, D.; Valentini, R.; Aubinet, M.; Bernhofer, C.; Knohl, A.; Laurila, T.; Lindroth, A.; Moors, E.; Pilegaard, K.; et al. Determinants of terrestrial ecosystem carbon balance inferred from European eddy covariance flux sites. *Geophys. Res. Lett.* **2007**, *34*, L01402. [[CrossRef](#)]
18. van der Molen, M.; Dolman, A.; Ciais, P.; Eglin, T.; Gobron, N.; Law, B.; Meir, P.; Peters, W.; Phillips, O.; Reichstein, M.; et al. Drought and ecosystem carbon cycling. *Agric. For. Meteorol.* **2011**, *151*, 765–773. [[CrossRef](#)]

19. Huxman, T.E.; Smith, M.D.; Fay, P.A.; Knapp, A.K.; Shaw, M.R.; Loik, M.E.; Smith, S.D.; Tissue, D.T.; Zak, J.C.; Weltzin, J.F.; et al. Convergence across biomes to a common rain-use efficiency. *Nature* **2004**, *429*, 651–654. [[CrossRef](#)]
20. Dai, A. Increasing drought under global warming in observations and models. *Nat. Clim. Chang.* **2013**, *3*, 52–58. [[CrossRef](#)]
21. Fu, Q.; Feng, S. Responses of terrestrial aridity to global warming. *J. Geophys. Res. Atmos.* **2014**, *119*, 7863–7875. [[CrossRef](#)]
22. Ciais, P.; Reichstein, M.; Viovy, N.; Granier, A.; Ogee, J.; Allard, V.; Aubinet, M.; Buchmann, N.; Bernhofer, C.; Carrara, A.; et al. Europe-wide reduction in primary productivity caused by the heat and drought in 2003. *Nature* **2005**, *437*, 529–533. [[CrossRef](#)]
23. Zeng, N.; Qian, H.; Roedenbeck, C.; Heimann, M. Impact of 1998–2002 midlatitude drought and warming on terrestrial ecosystem and the global carbon cycle. *Geophys. Res. Lett.* **2005**, *32*, L22709. [[CrossRef](#)]
24. Xiao, J.; Zhuang, Q.; Liang, E.; Shao, X.; McGuire, A.D.; Moody, A.; Kicklighter, D.W.; Melillo, J.M. Twentieth-Century Droughts and Their Impacts on Terrestrial Carbon Cycling in China. *Earth Interact.* **2009**, *13*, 1–31. [[CrossRef](#)]
25. Zhao, M.; Running, S.W. Drought-Induced Reduction in Global Terrestrial Net Primary Production from 2000 through 2009. *Science* **2010**, *329*, 940–943. [[CrossRef](#)]
26. Ma, Z.; Peng, C.; Zhu, Q.; Chen, H.; Yu, G.; Li, W.; Zhou, X.; Wang, W.; Zhang, W. Regional drought-induced reduction in the biomass carbon sink of Canada’s boreal forests. *Proc. Natl. Acad. Sci. USA* **2012**, *109*, 2423–2427. [[CrossRef](#)]
27. Chen, T.; Werf, G.R.; Jeu, R.A.M.; Wang, G.; Dolman, A.J. A global analysis of the impact of drought on net primary productivity. *Hydrol. Earth Syst. Sci.* **2013**, *17*, 3885–3894. [[CrossRef](#)]
28. Liu, Y.; Zhou, Y.; Ju, W.; Wang, S.; Wu, X.; He, M.; Zhu, G. Impacts of droughts on carbon sequestration by China’s terrestrial ecosystems from 2000 to 2011. *Biogeosciences* **2014**, *11*, 2583–2599. [[CrossRef](#)]
29. Vicente-Serrano, S.M.; Gouveia, C.; Camarero, J.J.; Beguería, S.; Trigo, R.; López-Moreno, J.I.; Azorín-Molina, C.; Pasho, E.; Lorenzo-Lacruz, J.; Revuelto, J.; et al. Response of vegetation to drought time-scales across global land biomes. *Proc. Natl. Acad. Sci. USA* **2013**, *110*, 52–57. [[CrossRef](#)] [[PubMed](#)]
30. He, W.; Ju, W.; Schwalm, C.R.; Sippel, S.; Wu, X.; He, Q.; Song, L.; Zhang, C.; Li, J.; Sitch, S.; et al. Large-Scale Droughts Responsible for Dramatic Reductions of Terrestrial Net Carbon Uptake Over North America in 2011 and 2012. *J. Geophys. Res. Biogeosci.* **2018**, *123*, 2053–2071. [[CrossRef](#)]
31. Granier, A.; Reichstein, M.; Bréda, N.; Janssens, I.; Falge, E.; Ciais, P.; Grünwald, T.; Aubinet, M.; Berbigier, P.; Bernhofer, C.; et al. Evidence for soil water control on carbon and water dynamics in European forests during the extremely dry year: 2003. *Agric. For. Meteorol.* **2007**, *143*, 123–145. [[CrossRef](#)]
32. Wei, X.; He, W.; Zhou, Y.; Ju, W.; Xiao, J.; Li, X.; Liu, Y.; Xu, S.; Bi, W.; Zhang, X.; et al. Global assessment of lagged and cumulative effects of drought on grassland gross primary production. *Ecol. Indic.* **2022**, *136*, 108646. [[CrossRef](#)]
33. Zhang, Z.; Ju, W.; Zhou, Y.; Li, X. Revisiting the cumulative effects of drought on global gross primary productivity based on new long-term series data (1982–2018). *Glob. Chang. Biol.* **2022**, *28*, 3620–3635. [[CrossRef](#)] [[PubMed](#)]
34. Na, L.; Na, R.; Bao, Y.; Zhang, J. Time-Lagged Correlation between Soil Moisture and Intra-Annual Dynamics of Vegetation on the Mongolian Plateau. *Remote Sens.* **2021**, *13*, 1527. [[CrossRef](#)]
35. Ye, C.; Sun, J.; Liu, M.; Xiong, J.; Zong, N.; Hu, J.; Huang, Y.; Duan, X.; Tsunekawa, A. Concurrent and Lagged Effects of Extreme Drought Induce Net Reduction in Vegetation Carbon Uptake on Tibetan Plateau. *Remote Sens.* **2020**, *12*, 2347. [[CrossRef](#)]
36. Barr, A.G.; Black, T.; Hogg, E.; Kljun, N.; Morgenstern, K.; Nestic, Z. Inter-annual variability in the leaf area index of a boreal aspen-hazelnut forest in relation to net ecosystem production. *Agric. For. Meteorol.* **2004**, *126*, 237–255. [[CrossRef](#)]
37. Krishnan, P.; Black, T.A.; Grant, N.J.; Barr, A.G.; Hogg, E.H.; Jassal, R.S.; Morgenstern, K. Impact of changing soil moisture distribution on net ecosystem productivity of a boreal aspen forest during and following drought. *Agric. For. Meteorol.* **2006**, *139*, 208–223. [[CrossRef](#)]
38. Mitchell, P.J.; O’Grady, A.P.; Pinkard, E.A.; Brodribb, T.J.; Arndt, S.K.; Blackman, C.J.; Duursma, R.A.; Fensham, R.J.; Hilbert, D.W.; Nitschke, C.R.; et al. An ecoclimatic framework for evaluating the resilience of vegetation to water deficit. *Glob. Chang. Biol.* **2016**, *22*, 1677–1689. [[CrossRef](#)]
39. Yi, C.; Ricciuto, D.; Li, R.; Wolbeck, J.; Xu, X.; Nilsson, M.; Aires, L.M.I.; Albertson, J.D.; Ammann, C.; Arain, M.A.; et al. Climate control of terrestrial carbon exchange across biomes and continents. *Environ. Res. Lett.* **2010**, *5*, 034007. [[CrossRef](#)]
40. Zhang, Y.; Gentile, P.; Luo, X.; Lian, X.; Liu, Y.; Zhou, S.; Michalak, A.M.; Sun, W.; Fisher, J.B.; Piao, S.; et al. Increasing sensitivity of dryland vegetation greenness to precipitation due to rising atmospheric CO₂. *Nat. Commun.* **2022**, *13*, 4875. [[CrossRef](#)]
41. Wang, Z.; He, Y.; Niu, B.; Wu, J.; Zhang, X.; Zu, J.; Huang, K.; Li, M.; Cao, Y.; Zhang, Y.; et al. Sensitivity of terrestrial carbon cycle to changes in precipitation regimes. *Ecol. Indic.* **2020**, *113*, 106223. [[CrossRef](#)]
42. Seddon, A.W.R.; Macias-Fauria, M.; Long, P.R.; Benz, D.; Willis, K.J. Sensitivity of global terrestrial ecosystems to climate variability. *Nature* **2016**, *531*, 229–232. [[CrossRef](#)]
43. Kanniah, K.D.; Beringer, J.; North, P.; Hutley, L. Control of atmospheric particles on diffuse radiation and terrestrial plant productivity A review. *Prog. Phys. Geogr.* **2012**, *36*, 209–237. [[CrossRef](#)]
44. Moore, C.E.; Beringer, J.; Evans, B.; Hutley, L.B.; McHugh, I.; Tapper, N.J. The contribution of trees and grasses to productivity of an Australian tropical savanna. *Biogeosciences* **2016**, *13*, 2387–2403. [[CrossRef](#)]
45. Ma, X.; Huete, A.; Moran, S.; Ponce-Campos, G.; Eamus, D. Abrupt shifts in phenology and vegetation productivity under climate extremes. *J. Geophys. Res. Biogeosci.* **2015**, *120*, 2036–2052. [[CrossRef](#)]
46. Knapp, A.K.; Carroll, C.J.W.; Denton, E.M.; La Pierre, K.J.; Collins, S.L.; Smith, M.D. Differential sensitivity to regional-scale drought in six central US grasslands. *Oecologia* **2015**, *177*, 949–957. [[CrossRef](#)] [[PubMed](#)]

47. Sims, D.A.; Brzostek, E.R.; Rahman, A.F.; Dragoni, D.; Phillips, R.P. An improved approach for remotely sensing water stress impacts on forest C uptake. *Glob. Chang. Biol.* **2014**, *20*, 2856–2866. [[CrossRef](#)]
48. Vicente-Serrano, S.M.; Beguería, S.; López-Moreno, J.I. A Multiscalar Drought Index Sensitive to Global Warming: The Standardized Precipitation Evapotranspiration Index. *J. Clim.* **2010**, *23*, 1696–1718. [[CrossRef](#)]
49. McKee, T.B.; Doesken, N.J.; Kleist, J. The relationship of drought frequency and duration to time scales. In Proceedings of the 8th Conference on Applied Climatology, Anaheim, CA, USA, 17–22 January 1993; Volume 17, pp. 179–183.
50. Liu, J.; Chen, J.; Cihlar, J.; Park, W. A process-based boreal ecosystem productivity simulator using remote sensing inputs. *Remote Sens. Environ.* **1997**, *62*, 158–175. [[CrossRef](#)]
51. Ju, W.; Gao, P.; Zhou, Y.; Chen, J.M.; Chen, S.; Li, X. Prediction of summer grain crop yield with a process-based ecosystem model and remote sensing data for the northern area of the Jiangsu Province, China. *Int. J. Remote Sens.* **2010**, *31*, 1573–1587. [[CrossRef](#)]
52. Feng, X.; Liu, G.; Chen, J.; Chen, M.; Liu, J.; Ju, W.; Sun, R.; Zhou, W. Net primary productivity of China's terrestrial ecosystems from a process model driven by remote sensing. *J. Environ. Manag.* **2007**, *85*, 563–573. [[CrossRef](#)]
53. Ju, W.; Gao, P.; Wang, J.; Zhou, Y.; Zhang, X. Combining an ecological model with remote sensing and GIS techniques to monitor soil water content of croplands with a monsoon climate. *Agric. Water Manag.* **2010**, *97*, 1221–1231. [[CrossRef](#)]
54. Liu, Y.; Zhou, Y.; Ju, W.; Chen, J.; Wang, S.; He, H.; Wang, H.; Guan, D.; Zhao, F.; Li, Y.; et al. Evapotranspiration and water yield over China's landmass from 2000 to 2010. *Hydrol. Earth Syst. Sci.* **2013**, *17*, 4957–4980. [[CrossRef](#)]
55. Liu, J.; Chen, J.M.; Cihlar, J.; Chen, W. Net primary productivity distribution in the BOREAS region from a process model using satellite and surface data. *J. Geophys. Res. Atmos.* **1999**, *104*, 27735–27754. [[CrossRef](#)]
56. Ju, W.; Chen, J.M.; Black, T.A.; Barr, A.G.; Liu, J.; Chen, B. Modelling multi-year coupled carbon and water fluxes in a boreal aspen forest. *Agric. For. Meteorol.* **2006**, *140*, 136–151. [[CrossRef](#)]
57. Sprintsin, M.; Chen, J.M.; Desai, A.; Gough, C.M. Evaluation of leaf-to-canopy upscaling methodologies against carbon flux data in North America. *J. Geophys. Res. Biogeosci.* **2012**, *117*, G01023. [[CrossRef](#)]
58. Zhang, F.; Chen, J.M.; Chen, J.; Gough, C.M.; Martin, T.A.; Dragoni, D. Evaluating spatial and temporal patterns of MODIS GPP over the conterminous U.S. against flux measurements and a process model. *Remote Sens. Environ.* **2012**, *124*, 717–729. [[CrossRef](#)]
59. Wang, Q.; Tenhunen, J.; Falge, E.; Bernhofer, C.; Granier, A.; Vesala, T. Simulation and scaling of temporal variation in gross primary production for coniferous and deciduous temperate forests. *Glob. Chang. Biol.* **2003**, *10*, 37–51. [[CrossRef](#)]
60. Matsushita, B.; Tamura, M. Integrating remotely sensed data with an ecosystem model to estimate net primary productivity in East Asia. *Remote Sens. Environ.* **2002**, *81*, 58–66. [[CrossRef](#)]
61. Zhang, F.; Ju, W.; Chen, J.; Wang, S.; Yu, G.; Li, Y.; Han, S.; Asanuma, J. Study on evapotranspiration in East Asia using the BEPS ecological model. *J. Nat. Resour.* **2010**, *25*, 1596–1606.
62. Chen, J.M.; Mo, G.; Pisek, J.; Liu, J.; Deng, F.; Ishizawa, M.; Chan, D. Effects of foliage clumping on the estimation of global terrestrial gross primary productivity. *Glob. Biogeochem. Cycles* **2012**, *26*, GB1019. [[CrossRef](#)]
63. He, Q.; Ju, W.; Dai, S.; He, W.; Song, L.; Wang, S.; Li, X.; Mao, G. Drought Risk of Global Terrestrial Gross Primary Productivity Over the Last 40 Years Detected by a Remote Sensing-Driven Process Model. *J. Geophys. Res. Biogeosci.* **2021**, *126*, e2020JG005944. [[CrossRef](#)]
64. Chen, J.M.; Ju, W.; Ciais, P.; Viovy, N.; Liu, R.; Liu, Y.; Lu, X. Vegetation structural change since 1981 significantly enhanced the terrestrial carbon sink. *Nat. Commun.* **2019**, *10*, 4259. [[CrossRef](#)] [[PubMed](#)]
65. Farquhar, G.D.; Von Caemmerer, S.; Berry, J.A. A biochemical model of photosynthetic CO₂ assimilation in leaves of C₃ species. *Planta* **1980**, *149*, 78–90. [[CrossRef](#)] [[PubMed](#)]
66. Chen, J.; Liu, J.; Cihlar, J.; Goulden, M. Daily canopy photosynthesis model through temporal and spatial scaling for remote sensing applications. *Ecol. Model.* **1999**, *124*, 99–119. [[CrossRef](#)]
67. Mo, X.; Chen, J.M.; Ju, W.; Black, T.A. Optimization of ecosystem model parameters through assimilating eddy covariance flux data with an ensemble Kalman filter. *Ecol. Model.* **2008**, *217*, 157–173. [[CrossRef](#)]
68. Parton, W.J.; Scurlock, J.M.O.; Ojima, D.S.; Gilmanov, T.G.; Scholes, R.J.; Schimel, D.S.; Kirchner, T.; Menaut, J.-C.; Seastedt, T.; Garcia-Moya, E.; et al. Observations and modeling of biomass and soil organic matter dynamics for the grassland biome worldwide. *Glob. Biogeochem. Cycles* **1993**, *7*, 785–809. [[CrossRef](#)]
69. Liu, Y.; Liu, R.; Chen, J.M. Retrospective retrieval of long-term consistent global leaf area index (1981–2011) from combined AVHRR and MODIS data. *J. Geophys. Res. Biogeosci.* **2012**, *117*, G04003. [[CrossRef](#)]
70. Lu, X.; Jiang, H.; Zhang, X.; Liu, J.; Zhang, Z.; Jin, J.; Wang, Y.; Xu, J.; Cheng, M. Estimated global nitrogen deposition using NO₂ column density. *Int. J. Remote Sens.* **2013**, *34*, 8893–8906. [[CrossRef](#)]
71. George, H.H.; Zohrab, A.S. Reference Crop Evapotranspiration from Temperature. *Appl. Eng. Agric.* **1985**, *1*, 96–99. [[CrossRef](#)]
72. Abramowitz, M.; Stegun, I.A. *Handbook of Mathematical Functions: With Formulas, Graphs, and Mathematical Tables (No. 55)*; Courier Dover Publications: Mineola, NY, USA, 1972.
73. Houghton, R. Why are estimates of the terrestrial carbon balance so different? *Glob. Chang. Biol.* **2003**, *9*, 500–509. [[CrossRef](#)]
74. Beguería, S.; Vicente-Serrano, S.M.; Angulo-Martinez, M. A Multiscalar Global Drought Dataset: The SPEIbase: A New Gridded Product for the Analysis of Drought Variability and Impacts. *Bull. Am. Meteorol. Soc.* **2010**, *91*, 1351–1356. [[CrossRef](#)]
75. Zang, C.S.; Buras, A.; Esquivel-Muelbert, A.; Jump, A.S.; Rigling, A.; Rammig, A. Standardized drought indices in ecological research: Why one size does not fit all. *Glob. Chang. Biol.* **2019**, *26*, 322–324. [[CrossRef](#)] [[PubMed](#)]

76. Slette, I.J.; Post, A.K.; Awad, M.; Even, T.; Punzalan, A.; Williams, S.; Smith, M.D.; Knapp, A.K. How ecologists define drought, and why we should do better. *Glob. Chang. Biol.* **2019**, *25*, 3193–3200. [[CrossRef](#)] [[PubMed](#)]
77. Law, B.; Falge, E.; Gu, L.; Baldocchi, D.; Bakwin, P.; Berbigier, P.; Davis, K.; Dolman, A.; Falk, M.; Fuentes, J.; et al. Environmental controls over carbon dioxide and water vapor exchange of terrestrial vegetation. *Agric. For. Meteorol.* **2002**, *113*, 97–120. [[CrossRef](#)]
78. Yu, G.-R.; Zhu, X.-J.; Fu, Y.-L.; He, H.-L.; Wang, Q.-F.; Wen, X.-F.; Li, X.-R.; Zhang, L.-M.; Zhang, L.; Su, W.; et al. Spatial patterns and climate drivers of carbon fluxes in terrestrial ecosystems of China. *Glob. Chang. Biol.* **2012**, *19*, 798–810. [[CrossRef](#)]
79. Guo-Dong, S. Sensitivity of the Terrestrial Ecosystem to Precipitation and Temperature Variability over China. *Atmos. Ocean. Sci. Lett.* **2014**, *7*, 382–387. [[CrossRef](#)]
80. Xu, L.; Baldocchi, D.D.; Tang, J. How soil moisture, rain pulses, and growth alter the response of ecosystem respiration to temperature. *Glob. Biogeochem. Cycles* **2004**, *18*, GB4002. [[CrossRef](#)]
81. Myneni, R.B.; Hall, F.G.; Sellers, P.J.; Marshak, A.L. The interpretation of spectral vegetation indexes. *IEEE Trans. Geosci. Remote Sens.* **1995**, *33*, 481–486. [[CrossRef](#)]
82. Tucker, C.J. Red and photographic infrared linear combinations for monitoring vegetation. *Remote Sens. Environ.* **1979**, *8*, 127–150. [[CrossRef](#)]
83. Ji, L.; Peters, A.J. Assessing vegetation response to drought in the northern Great Plains using vegetation and drought indices. *Remote Sens. Environ.* **2003**, *87*, 85–98. [[CrossRef](#)]
84. Zhang, T.; Xu, M.; Xi, Y.; Zhu, J.; Tian, L.; Zhang, X.; Wang, Y.; Li, Y.; Shi, P.; Yu, G.; et al. Lagged climatic effects on carbon fluxes over three grassland ecosystems in China. *J. Plant Ecol.* **2015**, *8*, 291–302. [[CrossRef](#)]

Disclaimer/Publisher’s Note: The statements, opinions and data contained in all publications are solely those of the individual author(s) and contributor(s) and not of MDPI and/or the editor(s). MDPI and/or the editor(s) disclaim responsibility for any injury to people or property resulting from any ideas, methods, instructions or products referred to in the content.